Fracture toughness of ABS additively manufactured by FDM process

O. Aourik*, M. Othmani, B. Saadouki, Kh. Abouzaid, A. Chouaf *

Laboratory of Control and Mechanical Characterization of Materials and Structures,
National Higher School of Electricity and Mechanics, Hassan II University of Casablanca,
B.P 8118 Oasis, Casablanca, Morocco
* Corresponding e-mail address: oumaima.aourik@ensem.ac.ma; a.chouaf@ensem.ac.ma
ORCID identifier: https://orcid.org/0000-0002-7451-5213 (O.A.)

ABSTRACT

Purpose: The purpose on this article is to study the failure of FDM printed ABS by exhibiting an exhaustive crack growth analysis mainly based on raster angle parameter.

Design/methodology/approach: Two approaches have been developed in this study; On one hand, mechanical experiments were carried out to determine the critical stress intensity factor K_{IC}. On the other hand, numerical analysis was used to predict the paths within the part as well as the crack propagation.

Findings: This work has clearly shown the effect of raster angle on the damage mechanism of the ABS printed by FDM. Indeed, for the combination 1 (0°/90°), the structure presents an important stiffness and a high degree of stress distribution symmetry with respect to the notch. Moreover, the crack propagation is regular and straight, and the damage surfaces are on the same plane. However, for the combination 2 (-45°/45°), the structure is less resistant with an asymmetrical stress distribution according to two different planes.

Research limitations/implications: In order to present an exhaustive study, we focused on the effect of two raster angles (including 0°/90°, -45°/45°) on the ABS crack propagation, additively manufactured. This study is still in progress for other raster angles, and will be developed from a design of experiments (DoE) design that incorporates all relevant factors. To highlight more the cracking mechanisms, microscopic observations will be developed in more depth.

Practical implications: Our analysis can be used as a decision aid in the design of FDM parts. Indeed, we can choose the raster angle that would ensure the desired crack propagation resistance for a functional part.

Originality/value: In this article, we have analyzed the mechanism of damage and crack propagation. This topic represents a new orientation for many research papers. For our study, we accompanied our experimental approach with an original numerical approach. In this numerical approach, we were able to mesh distinctly raster by raster for all layers.

Keywords: FDM, Raster angle, ABS, Tenacity, Damage, Simulation

ANALYSIS AND MODELLING

Research paper

1. Introduction

Over the past decade, a revolution in traditional manufacturing processes is being considered at the industrial level, ranging from functional prototyping applications to tool production, and finally, to product development. The term "additive manufacturing (AM)" refers to the set of three-dimensional printing techniques that appeared in the 1980s and were subsequently developed by manufacturers to keep pace with the evolution of the industry, and which are progressively gaining acceptance in key sectors such as automotive, aerospace and medical [1,2].

Considering the statistical data, the research sector related to the AM has increased by 40% from 2015 to 2019, which indicates that 3D printing is a growing manufacturing method. Medical, engineering, aerospace, automotive marketing and enterprises are mainly the industries benefiting from the development of 3D printing [3,4]. Therefore, 3D printing can meet the new needs of customers and generate revenue for companies [5].

Compared to other 3D printing methods, the one based on fused deposition modeling (FDM) has gained popularity due to its high prototyping capabilities, low initial investment, direct fabrication of complex structures, reduced waste maintenance costs, and availability of low-cost materials [6].

Among the most widely used thermoplastic materials in industries, we find the Acrylonitrile Butadiene Styrene (ABS) [7-9], which has a wide processing window and can be processed on most standard machines. It can be injection molded, blow molded or extruded. Its low melting temperature makes it particularly suitable for processing by 3D printing on an FDM machine.

Compared to conventional manufacturing processes, many studies have identified the scope of application of AM using the 3D printing process from the polymer filament. FDM is characterized by many process parameters that affect the quality of the obtained parts as well as their performance and mechanical properties [10-12]. This highlights the importance of studying the mechanical strength of FDM printed parts, as well as the effect of manufacturing parameters on the mechanical behavior of these components. With many printing parameters available, the advantage will be to know to better understand the mechanical response of these compact materials in tension. Some of these parameters include, layer height [13], perimeter, build orientation, infill pattern, infill density and raster angle [14]. In this regard, many studies have been developed [9,15]. Lubombo et al. [16] studied the influence of the type of infill pattern on the stiffness and strength of 3D printed cellular PLA parts. Yadav et al. adopted an experimental method to analyze and observe the two parameters, namely the infill pattern (rectilinear and gyroid) and the build orientation of the part, which affect the mechanical strength of the parts [17].

Through all these studies, we have noticed that the aspects of damage and cracking are not sufficiently studied especially by developing numerical simulations of this type of phenomenon. In present article, these aspects have particularly highlighted, we have therefore developed axes that allow us to understand the damage mechanism of parts obtained by 3D printing in ABS. To do this, we have mainly based on the impact of the raster angle on the fracture resistance of SENT specimens, taking inspiration from several works in the literature such as Jungivala et al., Hart et al. and Patel et al. [18-20], which confirm that the orientation of individual tracks of deposited material relative to the crack tip appears to have the most pronounced role in altering the fracture toughness of ABS made by FDM. Two approaches have been developed in this paper. The first one is experimental and based on tensile tests to determine the critical stress intensity factor K_{IC} and the second one is numerical by using the Von Mises stress distribution to highlight the possible crack propagation paths in this type of structure.

2. Fabrication of test specimens and testing

In this paper, manufacturing specimens from a virtual model until printing operation was investigated. CAD model should be converted to STereo-Lithography (STL) format which is a surface tessellation model that consists of an irregular mesh corresponding to the curved surfaces of the model. It is converted into a set of machine instructions describing the paths into the estimated printed part [21]. We have made two types of specimens according to the standards. Dogbone specimens (ISO 527-1 standard) [22] for material characterization and SENT (Single Edge Nibble Transmission) specimens (ISO 13586 and ASTM D5045 standard) [23,24] for the determination of the critical stress intensity factor K_{IC}.

Both types of specimens were produced by the FDM process using a RAISE 3D printer equipped with a 0.4 mm diameter extruder (see Fig. 1).

In order to print the specimens, one parameter was varied, which is the notch length. All other parameters such as print speed, filament diameter, and infill percentage are kept fixed (Tab. 1).
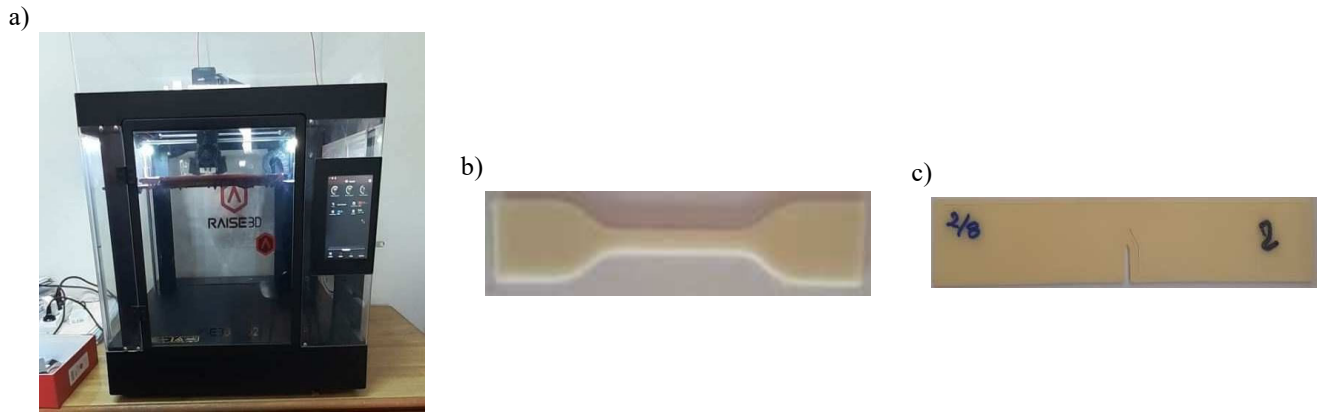
O. Aourik, M. Othmani, B. Saadouki, Kh. Abouzaid, A. Chouaf

a)

b)

c)

Fig. 1. a) RAISE 3D printer, b) Dogbone test specimens and c) SENT test specimens

Table 1.

Printing parameters of the dogbones

Parameters	Values	Units
Layer thickness	0.2	mm
First layer printing speed	30	mm/s
Print speed of other layers	150	mm/s
Raster angle	0 / 90	Deg
Infill percentage	90	%
Number of perimeters	2	
Fill type	Rectilinear	
Temperature	230	°C

For dogbone-shaped specimens (Fig. 2), specimen dimensions are selected in accordance with ISO 527-1 [22], using a single set of parameters including a layer thickness of 0.2 mm, a fill percentage of 90% with a raster angle of (0°/90°) (Tab. 1).
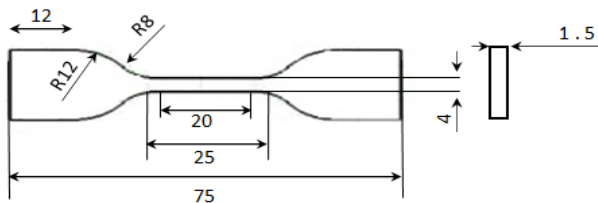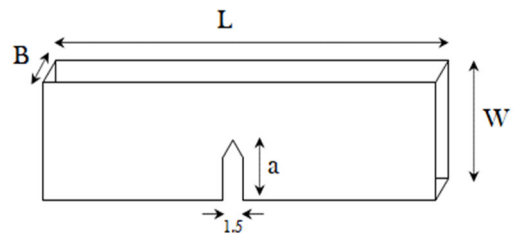

Fig. 2. Dimensions of the dogbone test specimen ISO 527-1

SENT samples was performed in several steps. First, the shape and dimensions of these samples according to the standards [23-25] was specified. The dimensions of the conceded samples are shown in Figure 3. For these samples, four crack lengths were studied as well as two raster patterns. In this study, we were interested to two combinations, crossing layers with -45°/45° and 0°/90° of raster angle.

Parameters	Values, mm
L	100
W	20
B	1.5
a	4, 6, 8, 10

Fig. 3. Dimensions of the SENT test specimen ISO 13586 and ASTM D5045

In order to avoid any accidental damage of the filaments, we recall that the geometrical model that allowed us to realize these specimens by FDM includes the notch. After obtaining the specimens, we manually initiated the crack at the root of the notch for the two conceded combinations (Tab. 2).

Table 2.

SENT specimen printing parameters for both combinations

Factors	Layer thickness, mm	Raster angle, °	Number of perimeters	Notch lengths, mm
Combination 1	0.2	0°/90°	2	4, 6, 8, 10
Combination 2	0.3	-45°/45°	3	4, 6, 8, 10

From the two types of specimens mentioned above, we therefore carried out our tensile tests for the characterization of the material and the determination of the toughness. To do this, we used a machine type DELTALAB which has

a maximum load of 50 kN, and a displacement of 0.01 mm/s (Fig. 4).

Fig. 4. Tensile test device "DELTALAB"

3. Characterization of ABS obtained by FDM

Pure ABS is considered one of the first and main materials used in manufacturing by FDM technology. To better analyze the damage of an ABS sample obtained by FDM, it is necessary to perform a basic mechanical characterization based on the tensile tests of dogbone samples, and extract the main mechanical characteristics (Fig. 5a), such as Young's modulus and yield strength

mentioned in Table 3. In addition, we extracted from the stress-strain curve of the ABS filament (Fig. 5b) [26,27], the constitutive law that will be introduced later in our numerical simulations.

Table 3.
Mechanical properties of ABS manufactured by FDM

Mechanical properties	Young's modulus, GPa	Elastic limit, MPa	Breaking stress, MPa	Breaking strain, %
Printed ABS test specimen	2.00	16.74	20.75	1.74

According to these results, the yield strength of printed ABS is 16.74 MPa. This value will be taken into consideration when we analyze the tensile test results of the SENT specimens.

The tensile tests on the SENT specimens allowed us to obtain the curves represented in Figures 6 and 7. Through these curves, it can be clearly seen that the notch affects the strength of the specimens in both combinations of parameters. The values of the elastic limit are about 10.58 MPa for combination 1 (Fig. 6), and 8 MPa for combination 2 (Fig. 7). From these results, we can deduce that combination 1 seems to have better tensile strength compared to combination 2.

Comparing the two combinations (0°/90°) and (-45°/45°), we can see a very marked difference in the mechanical behavior. Indeed, the raster angle plays a significant role in the damage process of SENT samples, as we will specify in the following paragraphs.
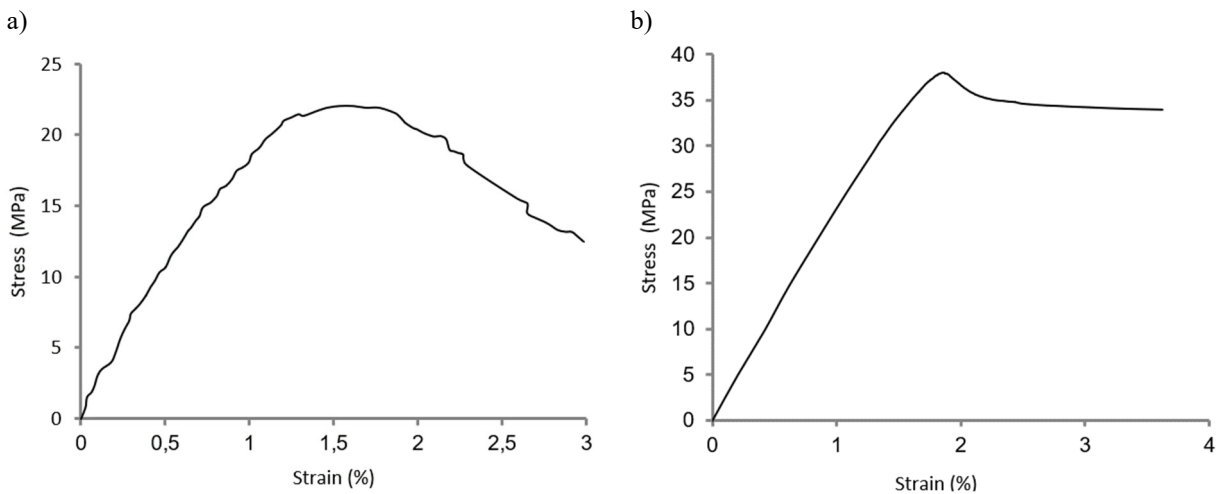
a)

b)

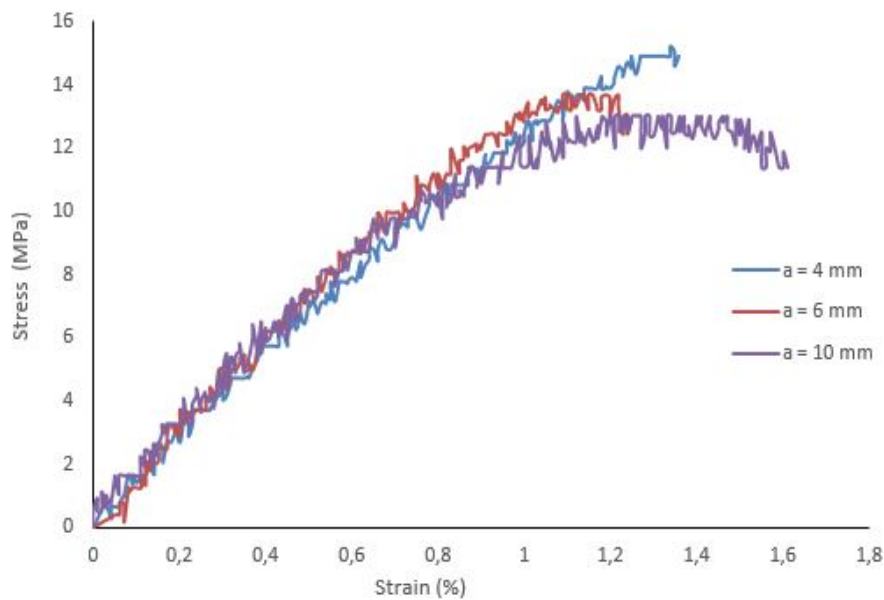Fig. 5. Stress-strain curves: a) ABS dogbone specimen obtained by FDM, b) ABS filament

Fig. 6. Tensile curves of test specimens of combination 1 (0°/ 90°) as a function of notch length a (4 mm, 6 mm and 10 mm)

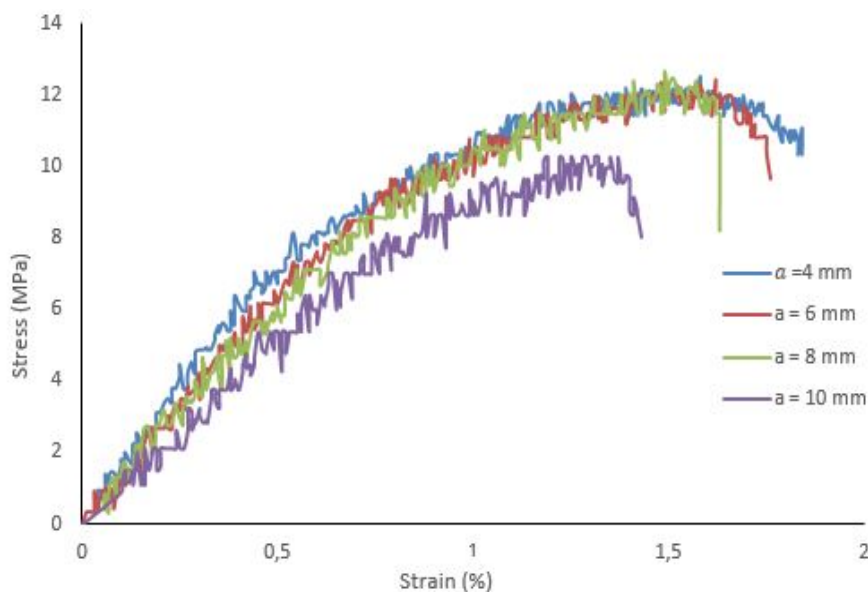Fig. 7. Tensile curve of test specimens of combination 2 (-45°/ 45°) as a function of notch length a (4 mm, 6 mm, 8 mm and 10 mm)

4. Determination of tenacity

From the results of experimental tests performed on simply notched specimens (SENT) (ISO 13586 and ASTM D5045), we determined for two distinct combinations the critical stress intensity factor K_{IC} that characterizes the strength.

To do this, we first determined the critical stress σ_c (Equation 1) from which the crack can propagate:

$$\sigma_c = \frac{F_Q}{S} \tag{1}$$

where F_Q is the crack initiation force and S (S= B*(W-a), Fig. 3) is the cross-sectional area of the specimen. And

finally, from this critical stress, we deduced the critical stress intensity factor by [28]:

$$K_{IC} = \sigma_C \cdot \sqrt{\pi a}\, f\left(\frac{a}{w}\right) \qquad (2)$$

In this equation (2), "a" is the length of the notch, W is the width of the specimen, and $f\left(\frac{a}{w}\right)$ is a geometric function given by [25,29]:

$$f\left(\frac{a}{w}\right) = 1.12 - 0.23\left(\frac{a}{w}\right) + 10.56\left(\frac{a}{w}\right)^2 - 21.74\left(\frac{a}{w}\right)^3 + 30.42\left(\frac{a}{w}\right)^4 \qquad (3)$$

According to the evolution of the curves of the two Figures 6 and 7, we can observe three phases in the behavior. For the first phase, the behavior is linear which corresponds to the elastic deformations of the filaments. In the second and third phases, the behavior is non-linear. Initially, there is a plastic deformation of the filaments with a slight increase in the resistance. In a second stage, this resistance decreases significantly, which corresponds to the progressive advance of the crack until the final rupture. This propagation can occur more or less quickly depending on the length of the notch. The smaller the notch, the greater the resistance and the slower the propagation.

Applying the above approach, we determined from the curves (Fig. 6 and Fig. 7) the K_{IC} values for the two combinations studied. The results obtained are grouped in Table 4.

Table 4.
Critical stress intensity factor K_{IC} of printed ABS specimens

length of the notch "a", mm		4	6	8	10
K_{IC}, MPa·$m^{1/2}$	Combination 1 (0°/90°)	2.30	3.08	3.08	6.37
	Combination 2 (-45°/45°)	1.71	2.84	3.87	6.63

For each parameter combination, we obtained K_{IC} values ranging from 1.7 MPa·$m^{1/2}$ to 3.87 MPa·$m^{1/2}$ for notch lengths ranging from 4 mm to 8 mm. These values are of the same order of magnitude as those in the literature [30,31]. But for notch lengths greater than 8mm, the K_{IC} reaches values greater than 6 MPa·$m^{1/2}$. Indeed, from these long notch lengths we approach the perimeters of the specimen, which opposes a great resistance to the propagation of the crack.

Overall, from the results of this part of our study, we can deduce that combination 1 (0°/90°) generates a better resistance to crack propagation compared to combination 2 (-45°/45°), which has been confirmed by the work of McLouth et al. [32].

5. Numerical simulations

Based on all the experimental results and deduced conclusions, we related the resistance to crack propagation with the geometry of the structure, in particular the raster angle. To do this, we performed simulations of the behavior of the specimens with the notch in order to locate the stress concentration zones that can give an idea of the possible propagation paths of the crack.

In order to perform the numerical simulations in accordance with the FDM manufacturing method, a script in "Python", which is a programming language integrated in the "Abaqus Standard" calculation code, was developed. This script executes into "Abaqus Standard" all the instructions of the G-code file to draw the trajectories [33].

5.1. Geometric model and boundary conditions

To numerically analyze the mechanical strength of the virtual specimen, we considered a specimen that complies with the ISO 13586 standard. To prepare the virtual specimen for the static tensile test, we created 'Tie' type interaction contacts between every two successive layers of the specimen and between the filaments. Then we introduced, in the material part of Abaqus, the behavior law of the ABS filament (Fig. 5b) [26,27] from which we extracted the following characteristics: Young's modulus equal to 2.0 GPa, Poisson's ratio equal to 0.3 and density of 1050 Kg/m^3.

The boundary conditions applied during the numerical simulation are identical to those applied during a physical test. Thus, we imposed an embedding on one face of our virtual specimen while we imposed on the other face a forced displacement $u_0 = 4\, mm$ along the longitudinal axis. This value was obtained from our experimental tests on physical specimens.

For the mesh of the virtual specimen, we considered tetrahedral 3D linear elements, as can be seen in Figure 8 which shows an example of a SENT specimen obtained with combination 1 (0°/90°).

5.2. Stress distribution

From our numerical simulations, we have represented in Figure 9 the distribution of equivalent Von Mises stresses for the two combinations (0°/90°) and (-45°/45°) studied.
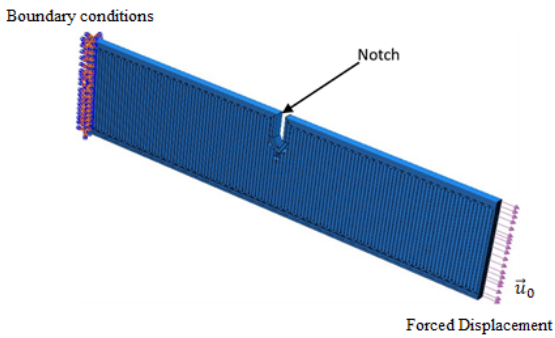
Fig. 8. Modeling of the SENT specimen obtained by FDM with the boundary conditions and the imposed displacement, in the case (0°/90°)

Through the maps of Figure 9, we can clearly observe a strong concentration of stresses in the vicinity of the notch due to the geometric discontinuity of the notch. This concentration differs from one combination to another.

For combination 1 (0°/90°), the concentration is symmetrical with respect to the notch. As the load increases, this concentration extends downward symmetrically. This is illustrated in Figure 10a, showing a cross-sectional plane of the specimen in which, it can be seen that the stress concentration is well distributed symmetrically across the width. This distribution as well as the level of the Von Mises stress that exceeds the elastic limit of the printed specimen would partly condition the path of the crack propagation. For this combination (0°/90°) the crack path could only be straight, parallel to the crack plane and regular as shown by the fracture surfaces (see Fig. 10b) and the front view of the crack (see Fig. 10c).

In contrast, for combination 2 (-45°/45°), the stress concentration is not symmetrical as shown in Figure 9b and this is due to the raster angle. As the load increases, this asymmetry changes with the advancement of the crack by changing the areas of high concentration from one side to the other with respect to the axis of symmetry of the notch.
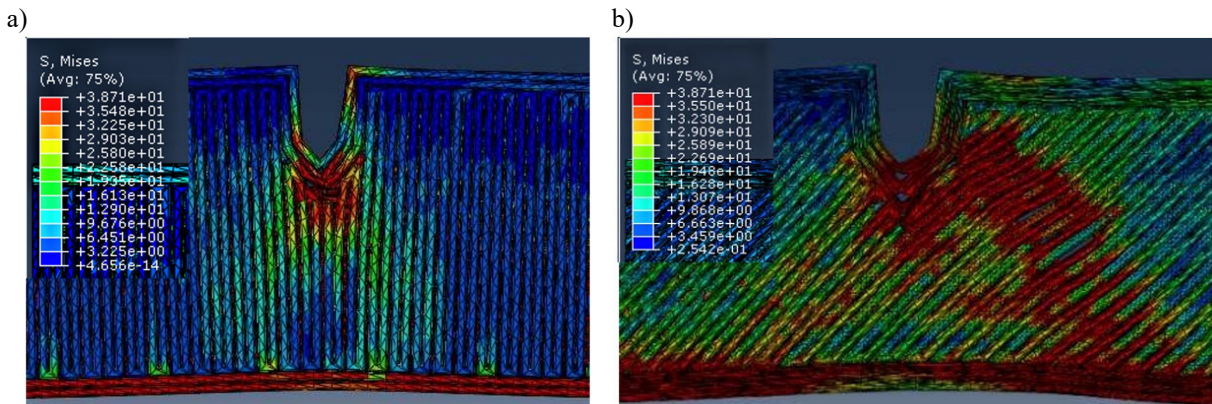

Fig. 9. Distribution of Von-Mises stresses in the vicinity of the notch, a) combination 1(0°/90°), b) combination 2(-45°/45°)
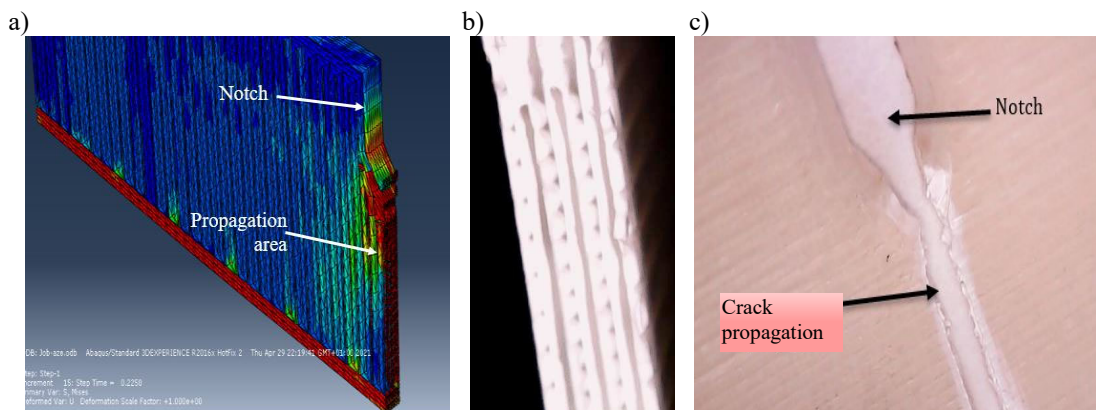

Fig. 10. Combination 1 (0°/90°): a) Von Mises stress distribution, b) fracture facies and c) right crack

a)   b)   c)
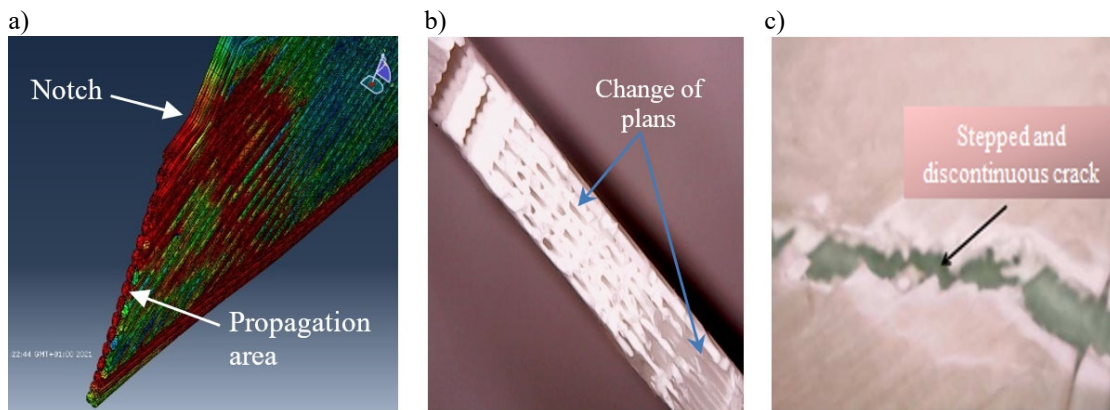
Fig. 11. Combination 2 (-45°/+45°): a) Von Mises stress distribution, b) fracture facies and c) crack bifurcation

With this change of stress concentration zone, the crack propagates with very marked bifurcations as shown by the fracture surface (Fig. 11b) and the frontal view of the crack (Fig. 11c). The fracture surface (Fig. 11b) clearly shows that the crack changes plane as it advances. The rugged crack path is clearly seen in the front view (Fig. 11c).

The previous results are almost in respect to those obtained by Isaac et al [34]. They observed that, for a raster angle of (0°/90°), the crack propagated symmetrically along the axis of the notch. On the other hand, for a raster angle of (-45°/+45°), the crack growth evolved along with the -45°/+45° directions in an asymmetrical manner.

For both combinations studied, the crack propagation plane follows the path of least resistance of the unaligned filaments, as previously mentioned by Zaldivar et al [35]. For the combination (0°/90°) the aligned filaments, which are perpendicular to the propagation plane, act as strong barriers to crack propagation.

As result, the first combination (0°/90°) is recommended due to the best mechanical properties that present including resistance and toughness.

6. Conclusions

In this study, experimental and numerical analysis to determine the damage mechanism of 3D printing ABS have been developed by studding the effect of the raster angle on the crack propagation.

For K_{IC}, the values obtained ranged from 1.7 MPa·m$^{1/2}$ to 3.87 MPa·m$^{1/2}$. These values are in respect to the literature. Comparing the two combinations studied, it can be seen that the combination generates a better resistance to crack propagation. This can be confirmed by comparisons of the tensile curves obtained from the tensile tests. The maximum

stress level of the combination (0°/90°) is higher than that of the combination (-45°/45°).

Numerical simulations have revealed high stress concentrations around the notch. This concentration differs from one combination to another. For combination 1 (0°/90°), the concentration is symmetrical with respect to the notch and when the load increases, it extends downwards in a symmetrical manner. Indeed, on a cross-sectional plane of the specimen, the stress concentration is well distributed symmetrically across the width, which is in harmony with the crack growth path.

In contrast, for combination 2 (-45°/45°), the stress concentration is not symmetrical and this is due to the raster angle. As the load increases, this asymmetry changes by changing the areas of high concentration from one side to the other with respect to the axis of symmetry of the notch. Taking this observation into account, the crack propagation would follow a path with bifurcations as shown in the fracture surface.

Finally, a structure obtained by 3D printing in ABS with a combination 1 (0°/90°) presents a better mechanical resistance and a better toughness. Whereas, with a combination 2 (-45°/45°), the specimen is less resistant to crack propagation.

References

[1] Ł. Wiechetek, A. Gola, Agile Manufacturing and Commerce. The Impact of 3D Printing on Markets and Business Processes, Przedsiębiorczość i Zarządzanie 19/5(1) (2018) 99-116.

[2] V. Dhinakaran, K.P. Manoj Kumar, P.M. Bupathi Ram, M. Ravichandran, M. Vinayagamoorthy, A review on recent advancements in fused deposition modeling,

           O. Aourik, M. Othmani, B. Saadouki, Kh. Abouzaid, A. Chouaf

Materials Today: Proceedings 27/2 (2020) 752-756. DOI: https://doi.org/10.1016/j.matpr.2019.12.036

[3] T.J. Gordelier, P.R. Thies, L. Turner, L. Johanning, Optimising the FDM additive manufacturing process to achieve maximum tensile strength: a state-of-the-art review, Rapid Prototyping Journal 25/6 (2019) 953-971. DOI: https://doi.org/10.1108/RPJ-07-2018-0183

[4] M. Othmani, A. Chouaf, Kh. Zarbane, Kh. Abouzaid, M. Chergui, Mechanical strength of a part obtained by simulation of the FDM type additive manufacturing process, Proceedings of the 13th Mechanical Congress, Meknes, Morocco, 2017 (in French).

[5] G.D. Goh, S. Agarwala, G.L. Goh, V. Dikshit, S.L. Sing, W.Y. Yeong, Additive manufacturing in unmanned aerial vehicles (UAVs): challenges and potential, Aerospace Science and Technology 63 (2017) 140-151.
DOI: https://doi.org/10.1016/j.ast.2016.12.019

[6] S. Wickramasinghe, T. Do, P. Tran, FDM-based 3D printing of polymer and associated composite: A review on mechanical properties, defects and treatments, Polymers 12/7 (2020) 1529.
DOI: https://doi.org/10.3390/polym12071529

[7] T. Sathies, P. Senthil, M.S. Anoop, A review on advancements in applications of fused deposition modeling process, Rapid Prototyping Journal 26/4 (2020) 669-687. DOI: https://doi.org/10.1108/RPJ-08-2018-0199

[8] B. Rankouhi, S. Javadpour, F. Delfanian, T. Letcher, Failure analysis and mechanical characterization of 3D printed ABS with respect to layer thickness and orientation, Journal of Failure Analysis and Prevention 16/3 (2016) 467-481.
DOI: https://doi.org/10.1007/s11668-016-0113-2

[9] T. Letcher, B. Rankouhi, S. Javadpour, Experimental study of mechanical properties of additively manufactured ABS plastic as a function of layer parameters, Proceedings of the ASME 2015 International Mechanical Engineering Congress and Exposition, Volume 2A: Advanced Manufacturing. Houston, Texas, USA, 2015, V02AT02A018. DOI: https://doi.org/10.1115/IMECE2015-52634

[10] O.A. Mohamed, S.H. Masood, J.L. Bhowmik, Mathematical modeling and FDM process parameters optimization using response surface methodology based on Q-optimal design, Applied Mathematical Modelling 40/23-24 (2016) 10052-10073. DOI: https://doi.org/10.1016/j.apm.2016.06.055

[11] R. Kristiawan, F. Imaduddin, D. Ariawan, Ubaidillah, Z. Arifin, A review on the fused deposition modeling (FDM) 3D printing: Filament processing, materials, and printing parameters, Open Engineering 11/1 (2021) 639-649. DOI: https://doi.org/10.1515/eng-2021-0063

[12] D. Popescu, A. Zapciu, C. Amza, F. Baciu, R. Marinescu, FDM process parameters influence over the mechanical properties of polymer specimens: A review, Polymer Testing 69 (2018) 157-166. DOI: https://doi.org/10.1016/j.polymertesting.2018.05.020

[13] W. Wu, P. Geng, G. Li, D. Zhao, H. Zhang, J. Zhao, Influence of layer thickness and raster angle on the mechanical properties of 3D-printed PEEK and a comparative mechanical study between PEEK and ABS, Materials 8/9 (2015) 5834-5846. DOI: https://doi.org/10.3390/ma8095271

[14] I.J. Solomon, P. Sevvel, J. Gunasekaran, A review on the various processing parameters in FDM, Materials Today: Proceedings 37/2 (2021) 509-514. DOI: https://doi.org/10.1016/j.matpr.2020.05.484

[15] P.K. Mishra, P. Senthil, S. Adarsh, M.S. Anoop, An investigation to study the combined effect of different infill pattern and infill density on the impact strength of 3D printed polylactic acid parts, Composites Communications 24 (2021) 100605.
DOI: https://doi.org/10.1016/j.coco.2020.100605

[16] C. Lubombo, M.A. Huneault, Effect of infill patterns on the mechanical performance of lightweight 3D-printed cellular PLA parts, Materials Today: Communications 17 (2018) 214-228.
DOI: https://doi.org/10.1016/j.mtcomm.2018.09.017

[17] D.K. Yadav, R. Srivastava, S. Dev, Design and fabrication of ABS part by FDM for automobile application, Materials Today: Proceedings 26/2 (2020) 2089-2093.
DOI: https://doi.org/10.1016/j.matpr.2020.02.451

[18] D. Jungivala, P.K. Gurrala, Finite element analysis of fused filament extrusion build part using different build orientation, Materials Today: Proceedings 38/5 (2021) 3264-3268.
DOI: https://doi.org/10.1016/j.matpr.2020.10.010

[19] K.R. Hart, E.D. Wetzel, Fracture behavior of additively manufactured acrylonitrile butadiene styrene (ABS) materials, Engineering Fracture Mechanics 177 (2017) 1-13.
DOI: https://doi.org/10.1016/j.engfracmech.2017.03.028

[20] N.D. Patel, B.B. Patel, Fracture analysis of FDM manufactured acrylonitrile butadiene styrene using FEM, International Journal of Recent Research in Civil and Mechanical Engineering 2/1 (2015) 84-90.

[21] M. Othmani, Kh. Zarbane, A. Chouaf, Analysis of the porosity and mechanical behavior in compression of the abs parts obtained by the fused deposition modeling, Proceedings of the Moroccan Workshop on 3D Printing "MW3DP'19", Casablanca, Morocco, 2019.

[22] ISO 527-1:2012. Plastics – Determination of tensile properties – Part 1: General principles, International Organization of Standardization, Geneva, Switzerland, 2012.

[23] ISO 13586:2018. Plastics – Determination of Fracture Toughness (GIC and KIC) – Linear Elastic Fracture Mechanics (LEFM) Approach, International Organization for Standardization, Geneva, Switzerland, 2018.

[24] ASTM D5045-99. Standard Test Methods for Plane-Strain Fracture Toughness and Strain Energy Release Rate of Plastic Materials, ASTM International, West Conshohocken, PA, USA, 1999.
DOI: https://doi.org/10.1520/D5045-99

[25] H. Tada, P.C. Paris, G.R. Irwin, The analysis of cracks handbook, Third Edition, ASME Press, New York, 2000. DOI: https://doi.org/10.1115/1.801535

[26] A. Schmailzl, T. Amann, M. Glockner, M. Fadanelli, Finite element analysis of thermoplastic probes under tensile load using LS-DYNA compared to ANSYS WB 14 in correlation to experimental investigations, Proceedings of the ANSYS Conference and 30th CADFEM Users Meeting, Kassel, 2012, 1-10.

[27] M. Othmani, A. Chouaf, Kh. Zarbane, Modeling and numerical analysis of the mechanical behavior of parts obtained by the FDM type additive manufacturing process, Proceedings of the Mediterranean Symposium on Smart City Application "SCAMS'17", Tangier, Morocco, 2017, Article 3, 1-4.
DOI: https://doi.org/10.1145/3175628.3175654

[28] K. Abouzaid, S. Guessasma, S. Belhabib, D. Bassir, A. Chouaf, Printability of co-polyester using fused deposition modeling and related mechanical performance, European Polymer Journal 108 (2018) 262-273. DOI: https://doi.org/10.1016/j.eurpolymj.2018.08.034

[29] M. Zeleke, E. Dintwa, K.N. Nwaigwe, Stress intensity factor computation of inclined cracked tension plate using XFEM, Engineering Solid Mechanics 9/4 (2021) 363-376.
DOI: http://dx.doi.org/10.5267/j.esm.2021.7.002

[30] F. Ning, W. Cong, J. Qiu, J. Wei, S. Wang, Additive manufacturing of carbon fiber reinforced thermoplastic composites using fused deposition modeling, Composites Part B: Engineering 80 (2015) 369-378. DOI: https://doi.org/10.1016/j.compositesb.2015.06.013

[31] A.K. Sood, R.K. Ohdar, S.S. Mahapatra, Parametric appraisal of mechanical property of fused deposition modeling processed parts, Materials and Design 31/1 (2010) 287-295.
DOI: https://doi.org/10.1016/j.matdes.2009.06.016

[32] T.D. McLouth, J.V. Severino, P.M. Adams, D.N.Patel, R.J. Zaldivar, The impact of print orientation and raster pattern on fracture toughness in additively manufactured ABS, Additive Manufacturing 18 (2017) 103-109.
DOI: https://doi.org/10.1016/j.addma.2017.09.003

[33] M. Othmani, Kh. Zarbane, A. Chouaf, Enhanced mesostructural modeling and prediction of the mechanical behavior of acrylonitrile butadiene styrene parts manufactured by fused deposition modeling, International Review of Mechanical Engineering 14/4 (2020) 243-252.
DOI: https://doi.org/10.15866/ireme.v14i4.17736

[34] J.P. Isaac, S. Dondeti, H.V. Tippur, Crack initiation and growth in additively printed ABS: effect of print architecture studied using DIC, Additive Manufacturing 36 (2020) 101536.
DOI: https://doi.org/10.1016/j.addma.2020.101536

[35] R.J. Zaldivar, D.B. Witkin, T. McLouth, D.N. Patel, K.Schmitt, J.P. Nokes, Influence of processing and orientation print effects on the mechanical and thermal behavior of 3D-Printed ULTEM® 9085 Material, Additive Manufacturing 13 (2017) 71-80. DOI: https://doi.org/10.1016/j.addma.2016.11.007